Seasonality of westerly moisture transport in the East Asian summer monsoon and its implications for interpreting precipitation δ18O

Article

Published Version

AGU PUBLICATIONS

JGR

Journal of Geophysical Research: Atmospheres

RESEARCH ARTICLE
10.1002/2014JD022919

Key Points:
- Seasonal moisture source cycle for East Asian summer monsoon rainfall quantified
- Westerly transport drives EASM rainfall; easterly transport prevails in winter
- Strength of source effect in rainfall oxygen isotope ratios varies spatially

Supporting Information:
- Tables S1–S8
- Figure S1
- Figure S2
- Figure S3

Correspondence to:
A. J. Baker,
a.j.baker@durham.ac.uk

Citation:
Baker, A. J., H. Sodemann, J. U. L. Baldini, S. F. M. Breitenbach, K. R. Johnson, J. van Hunen, and P. Zhang (2015), Seasonality of westerly moisture transport in the East Asian summer monsoon and its implications for interpreting precipitation $\delta^{18}O$, *J. Geophys. Res. Atmos.*, *120*, 5850–5862, doi:10.1002/2014JD022919.

Received 4 DEC 2014
Accepted 20 MAY 2015
Accepted article online 25 MAY 2015
Published online 26 JUN 2015

Seasonality of westerly moisture transport in the East Asian summer monsoon and its implications for interpreting precipitation $\delta^{18}O$

Alexander J. Baker[1], Harald Sodemann[2], James U. L. Baldini[1], Sebastian F. M. Breitenbach[3], Kathleen R. Johnson[4], Jeroen van Hunen[1], and Zhang Pingzhong[5]

[1]Department of Earth Sciences, University of Durham, Durham, UK, [2]Geophysical Institute, University of Bergen, Bergen, Norway, [3]Department of Earth Sciences, University of Cambridge, Cambridge, UK, [4]Department of Earth System Science, University of California at Irvine, Irvine, California, USA, [5]School of Earth Sciences and Key Laboratory of Mineral Resources in Western China (Gansu Province), Lanzhou University, Lanzhou, China

Abstract East Asian summer monsoon (EASM) rainfall impacts the world's most populous regions. Accurate EASM rainfall prediction necessitates robust paleoclimate reconstructions from proxy data and quantitative linkage to modern climatic conditions. Many precisely dated oxygen isotope records from Chinese stalagmites have been interpreted as directly reflecting past EASM rainfall amount variability, but recent research suggests that such records instead integrate multiple hydroclimatic processes. Using a Lagrangian precipitation moisture source diagnostic, we demonstrate that EASM rainfall is primarily derived from the Indian Ocean. Conversely, Pacific Ocean moisture export peaks during winter, and the moisture uptake area does not differ significantly between summer and winter and is thus a minor contributor to monsoonal precipitation. Our results are substantiated by an accurate reproduction of summer and winter spatial rainfall distributions across China. We also correlate modern EASM rainfall oxygen isotope ratios with instrumental rainfall amount and our moisture source data. This analysis reveals that the strength of the source effect is geographically variable, and differences in atmospheric moisture transport may significantly impact the isotopic signature of EASM rainfall at the Hulu, Dongge, and Wanxiang Cave sites. These results improve our ability to isolate the rainfall amount signal in paleomonsoon reconstructions and indicate that precipitation across central and eastern China will directly respond to variability in Indian Ocean moisture supply.

1. Introduction

The East Asian summer monsoon (EASM) and Indian summer monsoon (ISM) are driven by both seasonal reversals in continent-ocean temperature gradients, which generate low-pressure anomalies over land, and seasonal shifts in mean tropical wind vectors [*Ding and Sikka*, 2006; *Molnar et al.*, 2010]. Rapid seasonal Hadley circulation reversal and cross-equatorial flow largely drive the onset of the extratropical EASM in June, coinciding with the boreal summer northward shift of the intertropical convergence zone (ITCZ), but frontal EASM precipitation extends farther north than the ITCZ [*Schneider et al.*, 2014]. These seasonal changes in atmospheric circulation cause warm, moisture-bearing air masses to migrate inland, engendering extreme wet seasons; approximately 80% of eastern China's total annual precipitation is received between May and August [*Webster et al.*, 1998]. ISM precipitation is derived from southerly transport from equatorial latitudes and subsequent westerly transport across the northern Indian Ocean into the Indian subcontinent. EASM precipitation is generated by convergence of southwesterly moisture transport, northward ITCZ shift, and easterly Pacific Ocean trade winds [*Liu et al.*, 2014]. However, the relative contributions of these transport mechanisms to precipitation across monsoonal China remain unquantified.

Reliable prediction of future EASM rainfall variability is a matter of considerable scientific and societal concern and depends upon the availability of robust paleoclimate reconstructions from high-resolution proxy archives [*Intergovernmental Panel on Climate Change* (*IPCC*), 2013], which place present-day monsoon trends in a longer-term context. In many paleomonsoon reconstruction studies, precipitation amount [*Wang et al.*, 2001; *Zhang et al.*, 2008] or monsoon intensity (summer-winter precipitation ratio) is inferred directly from absolute-dated stalagmite $\delta^{18}O$ records [*Cheng et al.*, 2009] based on a negative correlation between precipitation $\delta^{18}O$ and precipitation amount or rate (the "amount effect"), which is apparent in modern instrumental data, particularly from low-latitude regions [*Rozanski et al.*, 1992], albeit with

considerable spatial variability [*Johnson and Ingram*, 2004]. These proxy records track summer northern hemisphere insolation on millennial to glacial-interglacial time scales [*Cheng et al*., 2009] and evince monsoonal fluctuations in response to high-latitude climate change, particularly North Atlantic temperature [*Li et al*., 2014]. However, within the EASM region, disparate $\delta^{18}O$ trends have been reported from southern China [e.g., *Cosford et al*., 2008; *Hu et al*., 2008] and near to the northerly EASM limit [e.g., *Tan et al*., 2009; *Zhang et al*., 2008]. Potentially, such spatial heterogeneity in apparent precipitation patterns is evidence for a complex monsoon response to relatively moderate climate forcing. Therefore, using proxy $\delta^{18}O$ data to explicate past EASM dynamics requires a full understanding of the controls on $\delta^{18}O$ variability across monsoonal Asia.

Recent studies based on instrumental data [*Dayem et al*., 2010; *Johnson and Ingram*, 2004] and climate modeling [*Clemens et al*., 2010; *Liu et al*., 2014; *Pausata et al*., 2011] demonstrate that local and mesoscale processes cause spatiotemporal variability in $\delta^{18}O$-climate correlations. Specifically, these studies present evidence for a strong response of precipitation $\delta^{18}O$ within monsoonal China to upstream depletion during atmospheric moisture transport from tropical oceanic sources rather than to local rainfall variability exclusively [*Liu et al*., 2014]. This highlights a critical challenge for paleomonsoon reconstructions: the need to isolate the precipitation amount signal from other processes which affect precipitation (and therefore stalagmite) $\delta^{18}O$. Moreover, reconciling mismatches between stalagmite $\delta^{18}O$ and other terrestrial proxy paleoprecipitation records from China (e.g., magnetic susceptibility records from loess-paleosol successions) necessitates quantitative interpretations of stalagmite $\delta^{18}O$ [*Maher and Thompson*, 2012].

Numerous studies [e.g., *Breitenbach et al*., 2010; *Clemens et al*., 2010; *Sodemann et al*., 2008a] demonstrate that moisture source seasonality plays an important role in precipitation $\delta^{18}O$ variability by determining the initial evaporation conditions and, subsequently, the isotopic evolution of air parcels during moisture transport [*Sodemann et al*., 2008a]. At present, Lagrangian models are ideally suited to obtaining detailed, quantitative moisture source information at the spatial and temporal scales appropriate for comparison with observational precipitation $\delta^{18}O$ data. In this paper, we quantitatively investigate two critical yet poorly understood controls on Chinese precipitation $\delta^{18}O$: (i) present-day precipitation moisture source region variability and (ii) the seasonal characteristics of moisture transport. We then discuss their implications for developing accurate, quantitative paleomonsoon reconstructions.

2. Data and Methods

2.1. Lagrangian Moisture Source Diagnostic

We characterized the moisture origin of continental precipitation across central and eastern China quantitatively. This was achieved using a Lagrangian moisture source diagnostic [*Sodemann et al*., 2008b], which detects specific humidity changes along three-dimensional, kinematic backward trajectories of atmospheric air parcels delivering precipitation to a target area, thus quantifying the evaporative contributions of moisture sources to precipitation. The examined period is November 1999 to March 2005, which fully exploits the currently available data and is comparable in length to previous studies using this Lagrangian technique, which provided quantitative constraints on the modern moisture source climatology in disparate climate regions such as Greenland [*Sodemann et al*., 2008b], Belize [*Kennett et al*., 2012], the European Alps [*Sodemann and Zubler*, 2010], and Antarctica [*Sodemann and Stohl*, 2009]. Trajectories were computed with the widely used particle dispersion model FLEXPART (version 8.2) [*Stohl et al*., 2005] and in the simulation used for this study [*Stohl*, 2006], the global atmosphere was divided homogenously into 1.4 million particles, representing infinitesimal air parcels, each traced for 20 days using three-dimensional wind field data from the European Centre for Medium-Range Weather Forecasting operational analyses, available every 6 h at a $1° \times 1°$ horizontal resolution and at 60 vertical levels. Only trajectories delivering precipitation to a target area defined over China, the minimum (maximum) longitude and latitude of which are 95 (121)°E and 20 (40)°N, respectively (Figure 1), were considered. This target area is based on the known present-day spatial EASM precipitation distribution and encompasses the area influenced by the Meiyu Front, a stationary subtropical frontal system, which demarcates the mean northerly extent of the EASM (Figure 1). Additionally, we excluded areas whose elevation above mean sea level exceeds 2 km, such as the eastern Tibetan Plateau, to accurately isolate lowland regions of central and eastern China affected by the EASM. Based on air parcel latitude, longitude, altitude, pressure, and specific humidity output at each 6 h time step, the temporal

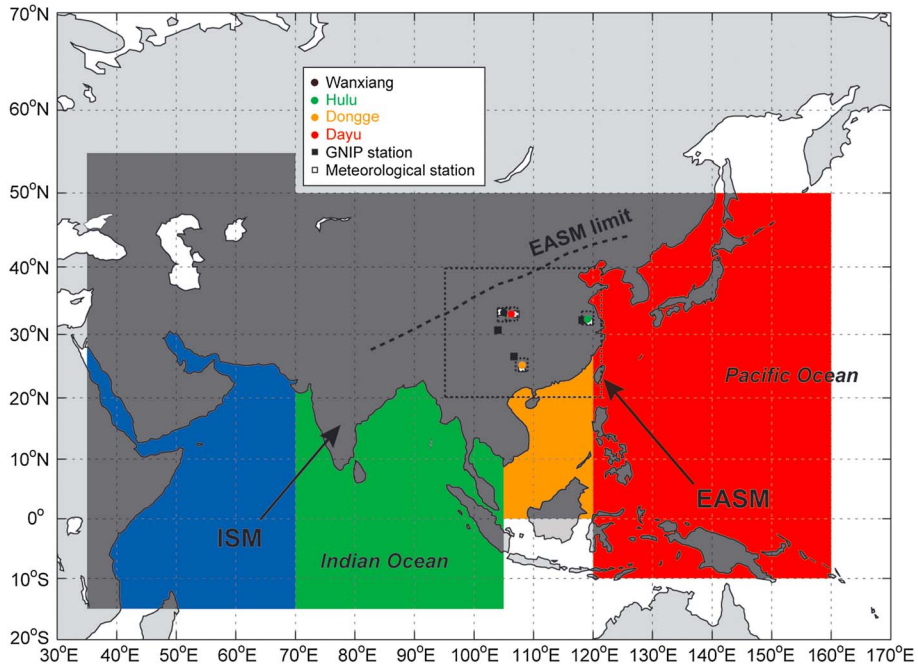

Figure 1. Target areas for precipitation moisture source diagnostic study (white dotted lines) and defined moisture source sectors: northwest Indian Ocean (blue), northeast Indian Ocean (green), South China Sea (orange), Philippine Sea (red), and terrestrial regions (dark grey). Sector color coding corresponds to Figure 7. Sectors were first demarcated by meridians and parallels; oceanic and land areas within each were subsequently separated, giving the source sectors shown (see supporting information). The black arrows indicate the traditionally assumed bulk transport direction of moisture masses in the tropical ISM and extratropical EASM subsystems based on mean boreal summer atmospheric pressure patterns. The GNIP (black markers) and meteorological stations (white markers) from which data were obtained for multivariate correlation analyses and the locations of each cave site discussed in the text are shown (color markers). Cave site colors correspond to those on Figure 8. For clarity, remaining land areas are shaded pale grey.

sequence of evaporation and precipitation was determined along the trajectory of each air mass precipitating within the target area using a threshold specific humidity criterion of 0.2 g kg^{-1} 6 h^{-1} to define moisture uptake and rainout. A full list of input parameters and values is given in Table S1 in the supporting information. From this along-trajectory sequence of uptake and rainout, and the relative contribution to air parcel moisture at each time step, a quantitative estimate of moisture source contributions is calculated, following *Sodemann et al.* [2008b]. Estimated Lagrangian precipitation is calculated from the specific humidity change in each trajectory during the 6 h before arrival at the target area.

Potential limitations to this Lagrangian method are (i) a weak sensitivity of the absolute moisture source strength to the threshold specific humidity criterion, which is minimized by considering specific humidity thresholds below 0.5 g kg^{-1} 6 h^{-1} [*James et al.*, 2004]; (ii) the assumption that evaporation and precipitation can be separated on a time scale of 6 h; (iii) and the inability to consider subgrid-scale moisture changes (e.g., due to evaporating precipitation). We assert that not accounting for subgrid-scale processes does not significantly afflict our study because modeled precipitation across central and eastern China reproduces an observational, 30 year precipitation climatology. There are important advantages to the Lagrangian approach. First, precipitation source regions are diagnosed quantitatively because the degree of local evaporation contribution to the total moisture in the air parcels is calculated. Previous studies have relied on trajectory end points [*Helsen et al.*, 2007] or the superposition of evaporation minus precipitation along trajectories [*James et al.*, 2004]. Second, direct evaporative moisture uptake is only diagnosed for a given air parcel if it is below the atmospheric boundary layer (ABL) at a point of specific humidity increase. Thereby, this method distinguishes evaporative moisture uptake originating within the ABL from moistening of air parcels in the free troposphere (FT), predominantly due to convective processes. By combining ABL and FT moisture contributions, we were able to attribute moisture sources to 93.5% of mean annual precipitation during 1999–2005 (Table S2 in the supporting information).

We quantified source signal variability in precipitation $\delta^{18}O$ (see supporting information) at cave sites in key locations (Figure 1): eastern China (Hulu Cave: 33°30′N, 119°10′E), southern China (Dongge Cave: 25°17′N, 108° 08′E), and near the northerly EASM limit (Wanxiang Cave: 33°19′N, 105°00′E; Dayu Cave: 33°08′N, 106°18′E). To achieve this, we ran the Lagrangian diagnostic with additional $2° \times 2°$ target areas centered on each selected cave site (Figure 1 and Table S3 in the supporting information). From the output for each target area, specific humidity-weighted mean monthly source longitude and latitude were computed. These data and precipitation amount data, obtained from nearby meteorological stations, were used as predictor variables in multivariate correlations with instrumental precipitation $\delta^{18}O$ data, obtained from the Global Network for Isotopes in Precipitation (GNIP) database [*International Atomic Energy Agency/World Meteorological Organization*, 2014]. For each cave site, we selected GNIP stations (Nanjing, Guiyang, and Chengdu, respectively) and meteorological stations (Hulu, Hechi, Wudu, and Hanzhong, respectively) that are both within or proximal to their respective target areas (Figure 1) and within the area of significant spatial precipitation correlation found by *Dayem et al*. [2010].

2.2. Moisture Source Sectorization

We divided continental Asia, the Philippine Sea, northern and low-latitude Indian Ocean, and the surrounding terrestrial and oceanic areas into 11 separate sectors (Table S3 in the supporting information) and determined the moisture contribution from each to precipitation within the regional and site-specific target areas. These raw, sectorized data are provided in Tables S4–S8 in the supporting information. ABL and FT moisture uptake data for individual sectors were further segregated into their constituent land and oceanic areas and used to compute the mean and total area-weighted contributions from four oceanic source regions and from terrestrial areas (Figure 1) to precipitation within monsoonal China during November 1999 to March 2005. These data not only establish the seasonality of eastward versus westward moisture advection but also help to characterize the importance of particular moisture source regions for proxy record sites by providing a way to quantify the strength of the source effect in precipitation $\delta^{18}O$. Therefore, this information may be used to better isolate the precipitation amount signal in $\delta^{18}O$-based paleomonsoon reconstructions.

3. Results and Discussion

3.1. Comparison of Lagrangian and Instrumental Precipitation Data

To first establish the credibility of the Lagrangian method adopted, we compared modeled and observational precipitation data: the seasonally composited precipitation modeled by the Lagrangian diagnostic was compared with the Global Precipitation Climatology Centre version 6 (GPCC6) data set [*Schneider et al*., 2011] for the climatological period of 1981–2010 (Figure 2). Precipitation amount within the target area is calculated from any specific humidity decrease during the final 6 h time step, following *Sodemann et al*. [2008b]. This Lagrangian precipitation estimate is generally biased high, which is a commonly observed characteristic due to neglecting the influence of cloud microphysics in generating model-derived precipitation [*Sodemann and Zubler*, 2010]. However, in this study the Lagrangian estimate compares favorably with the GPCC6 data. The mean seasonal Lagrangian precipitation captures the seasonal spatiotemporal distribution of rainfall across China accurately (Figure 2). The mean Lagrangian data for December to February show relatively high precipitation in southeast China and immediately northeast of the Himalaya compared with the GPCC6 data (Figure 2, December-January-February (DJF)). A similar spatial rainfall distribution is exhibited by both data sets during March-May, although the Lagrangian data do not capture the relatively low levels of precipitation in east India and peninsular Indochina during spring (Figure 2, March-April-May (MAM)). Data for June-August exhibit a well-defined gradient orientated WSW-ENE, likely representing the Meiyu Front [*Sampe and Xie*, 2010], and reproduce high monsoonal precipitation in northeast India (Figure 2, June-July-August (JJA)). During June to August, when ~80% of the total annual rainfall is received, the mean Lagrangian and GPCC6 precipitation values averaged over the target area are similar: 170 and 176 mm month^{-1}, respectively. Precipitation distribution and magnitude during September to November are also reproduced well (Figure 2, September-October-November (SON)). These Lagrangian precipitation data also reproduce GPCC6 precipitation averaged over our study period (November 1999 to March 2005), indicating that this period does not differ significantly from the mean spatiotemporal climatological precipitation distribution for central and eastern China

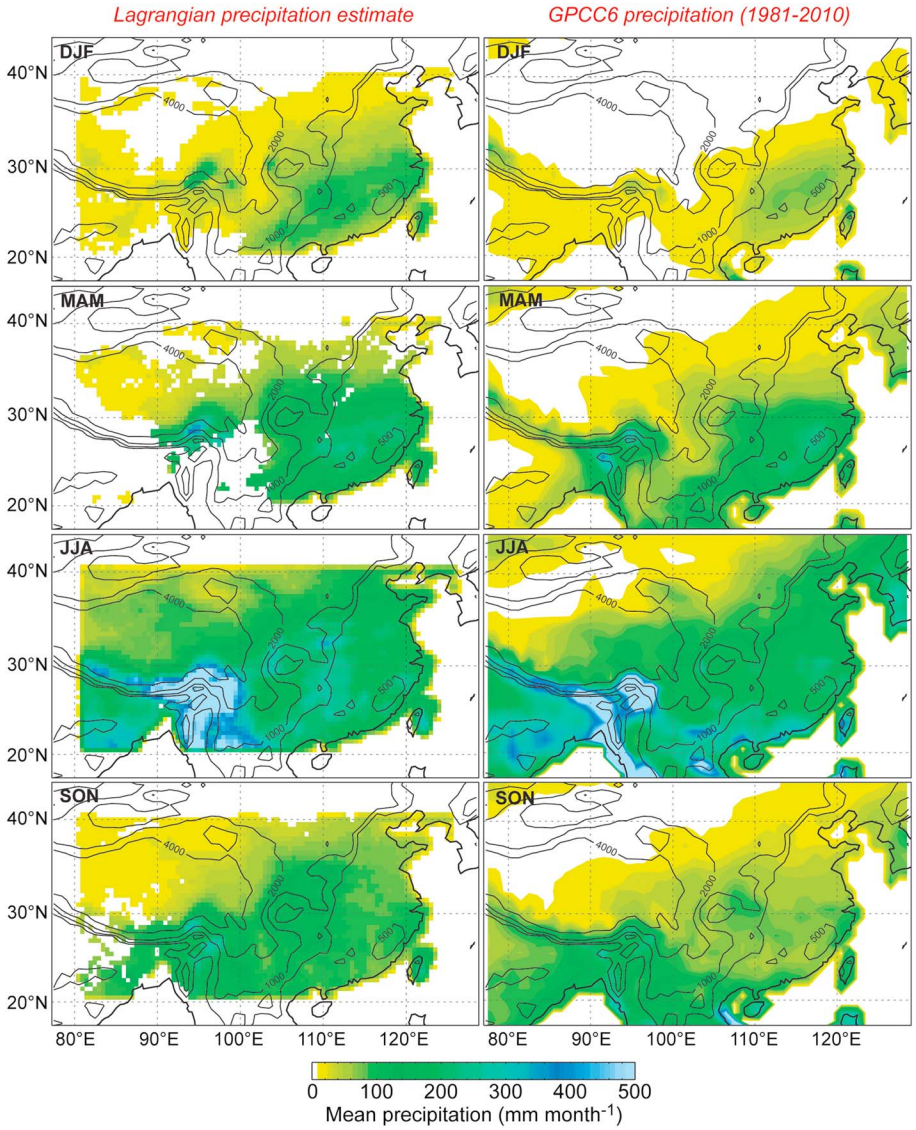

Figure 2. (left) Composited mean seasonal Lagrangian-estimated precipitation within China exhibit a close spatial and seasonal agreement with (right) Global Precipitation Climatology Centre version 6 (GPCC6) data [*Schneider et al.*, 2011]. These data were obtained from Deutscher Wetterdienst (available at www.dwd.de), and both data sets are averaged over December to February (DJF), March to May (MAM), June to August (JJA), and September to November (SON). Topographic contours (solid lines) are in meters above mean sea level.

(Figure S1 in the supporting information). Modeled precipitation is also in agreement with the globally gridded interpolation of precipitation monitoring observations of *Legates and Willmott* [1990] (not shown). These results establish the credibility of the Lagrangian method adopted in this study and firmly substantiate the diagnosed moisture source patterns for China discussed below.

3.2. EASM Moisture Source Patterns

The seasonal cycle of moisture sources of precipitation across monsoonal China shows a marked transition between a dry winter period, with easterly moisture contributions, and an intense summer monsoon phase, with extensive contributions from the northern Indian Ocean and moisture recycling over continental areas (Figure 3). During December to February, evaporative contributions of up to 15 mm month^{-1} occur principally over the western Philippine Sea, and relatively low evapotranspiration (up to 35 mm month^{-1}) is detected over southern China. The geographic extent of moisture uptake is relatively invariant over central China during these winter months, which is consistent with global oceanic

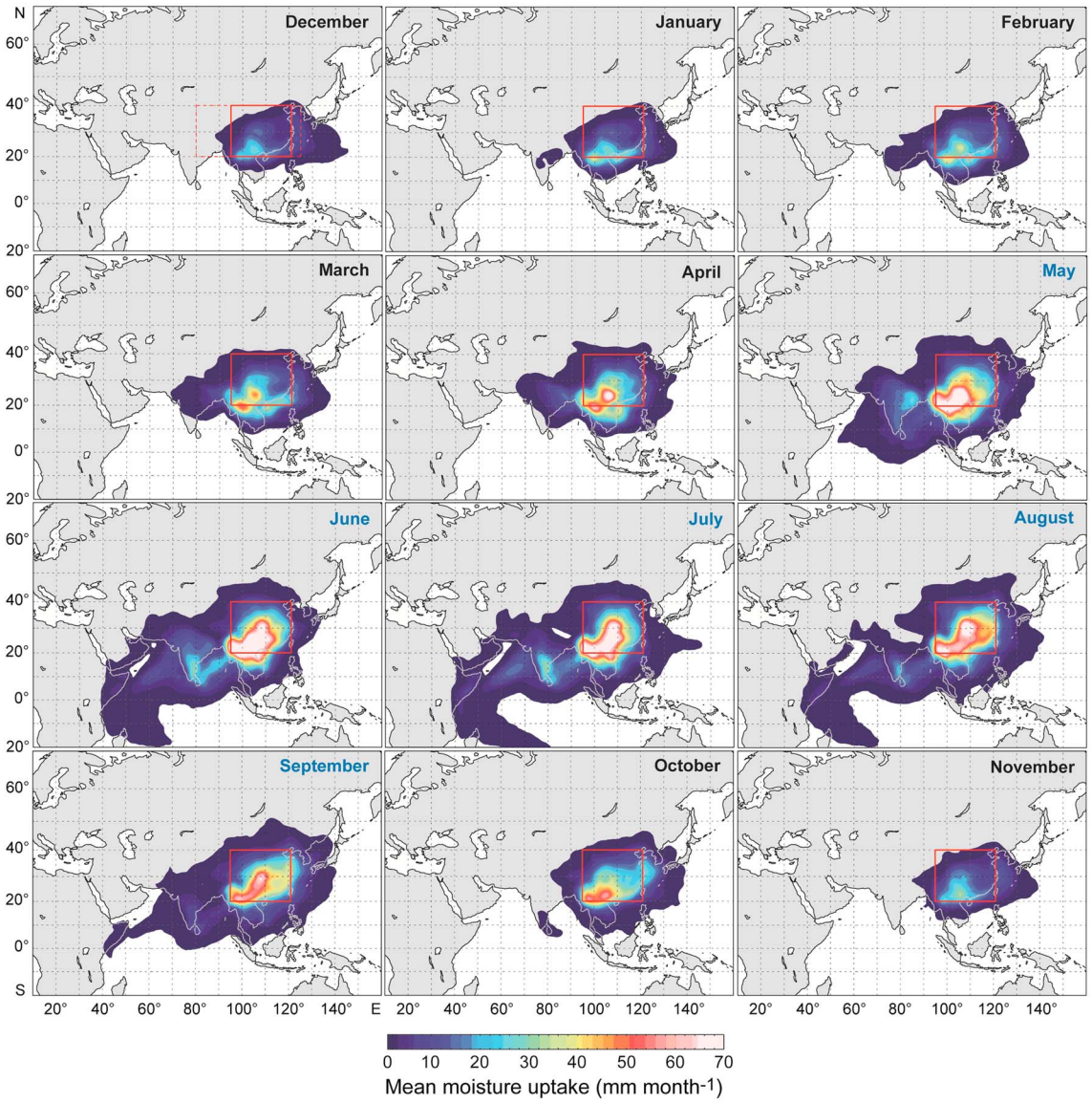

Figure 3. Mean monthly evaporative moisture uptake (within the ABL) contributing to precipitation across central and eastern China for the period of November 1999 to March 2005, showing mean precipitation within the target area (red box) projected back over its respective source locations. The EASM season is June to September; ASM months are in blue text. The area shown in Figures 5 and 6 is outlined in the December panel (red dashed box). Note that areas >2 km elevation were excluded from the Lagrangian model runs and numerical analyses.

evaporation simulations [*Gimeno et al.*, 2010; *van der Ent and Savenije*, 2013]. We note, however, that these studies are based on relatively idealized diagnostic methods (e.g., vertically integrated horizontal moisture fluxes). During March to April, prior to ISM onset, the moisture uptake region expands westward toward India, with ongoing uptake from the westernmost Philippine Sea. Greater evapotranspiration is detected over Bangladesh and northeast India, with additional contributions from the eastern Tibetan Plateau. Increased evaporation during ISM onset (May to June) is observed over the Bay of Bengal, substantiated by recent back trajectory results over comparably small target areas [*Breitenbach et al.*, 2010; *Chen et al.*, 2013; *Liu et al.*, 2011]. ISM onset also induces evaporation over the Arabian Sea, synchronous with the seasonal timing of increased latent heat supply to the Asian summer monsoon (ASM) from the equatorial and southern Indian Ocean and the associated lower troposphere moisture budget distributions [*Ding et al.*, 2004; *Martius et al.*, 2013]. Indian Ocean uptake extends westward and southward during EASM onset (June), following prevailing horizontal wind directions, which are also consistent with National Centers for Environmental Prediction/National Center for Atmospheric Research reanalysis 1000 hPa mean

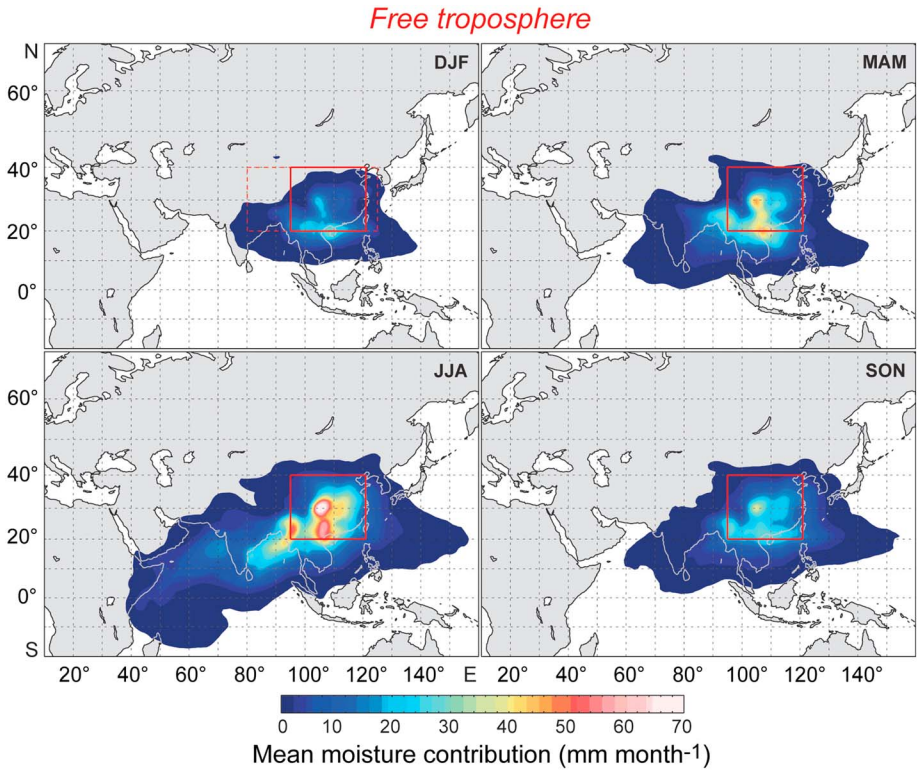

Figure 4. Mean seasonal free troposphere (above the ABL) moisture uptake contributing to precipitation within the regional target area (red box) from Lagrangian diagnostics for 1999–2005. The region shown in Figures 5 and 6 is outlined in the DJF panel (red dashed box).

wind vectors [*Clemens et al.*, 2010]. This uptake region develops during peak EASM (July to August) and recedes during the cessation of EASM precipitation over China (September). However, evaporation over the Philippine and South China Seas during the EASM is not markedly different from that during winter. The seasonal timing of this expansion and contraction behavior is also concurrent with the seasonal development and decay of the Siberian High. Evapotranspired moisture is primarily sourced from southern and eastern China and the Indian subcontinent during summer months. During the ASM, evapotranspiration contributes the greatest mean monthly uptake values (up to 70 mm month^{-1}), and recycled moisture does not fully recede to its dry winter state until November.

3.3. Free Troposphere Moisture Contributions

The Lagrangian diagnostic we use [*Sodemann et al.*, 2008b] distinguishes evaporative moisture uptake within the ABL from convective moistening of air parcels in the FT. Seasonally composited FT moisture contributions do not represent moisture sources directly because such moistening occurs above the ABL. Rather, these contributions represent convective moistening of air parcels, with shallow and deep convective detrainment of upper ABL moisture into the FT. The geographic distribution of the FT moisture contribution to precipitation within monsoonal China is similar to that of ABL uptake but exhibits a broader spatial pattern (Figure 4), particularly over the northern Indian Ocean, from which contributions are up to 40 mm month^{-1}. The area of moisture uptake from the northwest Pacific Ocean is present throughout the ASM season but represents a lower contribution (up to 10 mm month^{-1}) that is likely associated with the mean boreal summer position of the ITCZ.

During the ASM, two differences from direct evaporative contributions near the surface are identified: (i) the branch of Indian Ocean moisture contribution during June to August is significantly more expansive and (ii) a comparatively minor region of moistening is detected over the central Philippine Sea at ~20°N out to ~160°E during June to November.

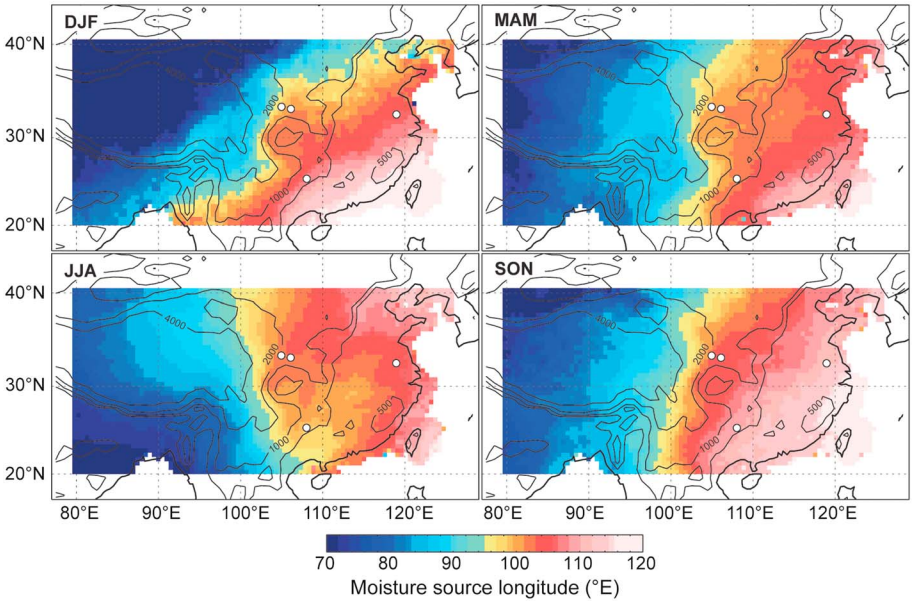

Figure 5. Mean seasonal source longitude of moisture masses responsible for precipitation within monsoonal China. Source longitude data are forward projected over the target area. Topographic contours (solid lines) are in meters above mean sea level. Summer precipitation within the target area is sourced from westerly longitudes, and this zonal moisture advection into eastern China is most intense during June (Figure S2 in the supporting information). Locations of selected cave sites are shown (white circles; see also Figure 1). Note that although areas >2 km elevation were excluded from the Lagrangian model runs and numerical analyses consistently, these forward projections show a larger data set which includes these areas for clarity.

3.4. Moisture Source Distribution Across Central and Eastern China

To characterize the spatial distribution of moisture sources across monsoonal China, we mapped Lagrangian forward projections of seasonal mean source longitude (Figure 5) and latitude (Figure 6) data. During December to February, source longitude exhibits a southeast-northwest gradient and shows a strong influence of the Westerlies in northwest China. We also observe areas where a topographic influence on moisture source distribution is apparent. The southeastern margin of the Tibetan Plateau, over the Ganges-

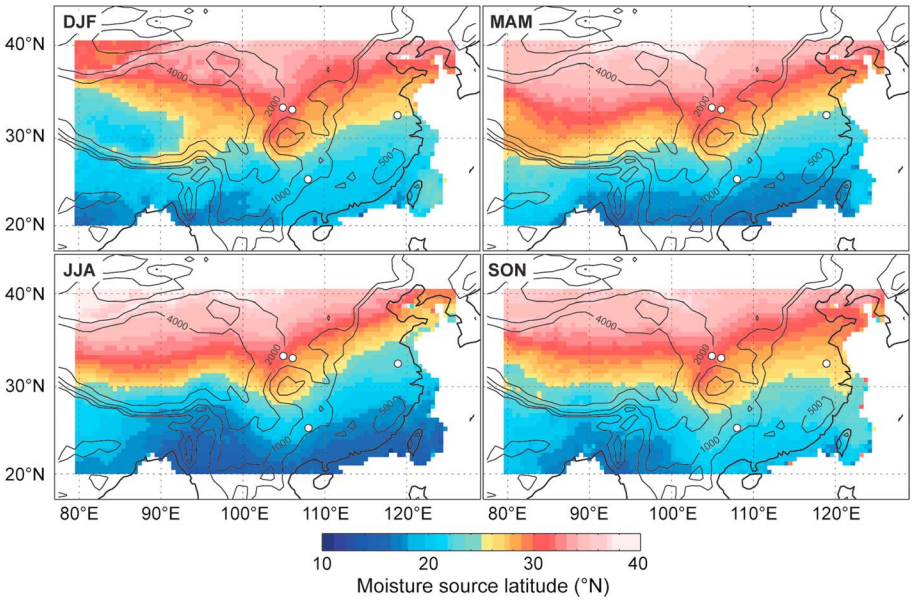

Figure 6. Mean seasonal source latitude of moisture masses responsible for precipitation within monsoonal China. Source latitude data are forward projected over the target area. Annotations are as per Figure 5.

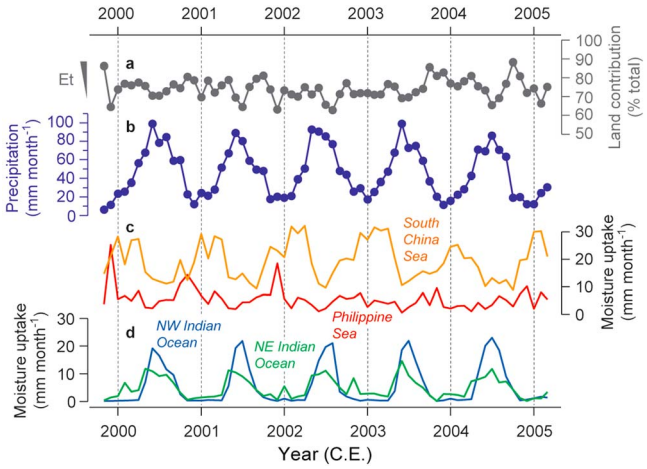

Figure 7. Time series of monthly (a) terrestrial moisture contribution to precipitation over the target area expressed as a percentage of total ABL uptake, (b) mean Lagrangian modeled precipitation over the target area, and total moisture contributions from (c) Pacific and (d) Indian Ocean source regions (see also Figure 1) to precipitation within monsoonal China. Indian Ocean and Pacific Ocean contributions exhibit opposite seasonality (see also Figure S3 in the supporting information). Data in Figure 7b are area weighted and show evaporative (ABL) uptake only, representing the evapotranspiration ("Et") signal. Data in Figures 7c and 7d are also area weighted but show combined ABL and FT moisture, giving the total contribution.

Brahmaputra deltaic region, and over the Chengdu basin, central China, each show graduation in source longitude which broadly follows topographic contours. During March to May, this axis of this winter gradient shifts to a meridional orientation, which is most marked between April and May (Figure S2 in the supporting information), representing incipient ISM onset. During May to August, monsoonal precipitation over eastern and southern China is sourced from relatively westerly locations (90°E–105°E), derived from the substantial Indian Ocean evaporation identified with the Lagrangian diagnostic (Figure 3). The winter southeast-northwest gradient resumes from October. Over the examined period, moisture source longitude variability at Hulu Cave (86°E–117°E), Dongge Cave (93°E–115°E), Wanxiang Cave (88°E–108 °E), and Dayu Cave (90°E–110°E) exceeds 20°.

Seasonal Lagrangian forward projections of moisture source latitude (Figure 6) exhibit a zonal gradient throughout the year, with precipitation sourced between 20 and 35°N during winter (December to February) and expanding to 10 and 40°N during peak EASM, again concurrent with the seasonal development and decay of the Siberian High. Within the target area, particularly in southern China, summer monsoonal precipitation is derived from a greater amount of moisture migrating from relatively southerly latitudes than winter precipitation, consistent with uptake maps (Figures 3 and 4). Moreover, summer moisture uptake occurs up to ~40°N, which represents increased evapotranspiration feeding recycled moisture to EASM precipitation. Over the examined period, moisture source latitude variability at Hulu Cave (20°N–33°N), Dongge Cave (17°N–25°N), Wanxiang Cave (27°N–36°N), and Dayu Cave (25°N–35°N) is less than that exhibited by source longitude data.

3.5. Moisture Transport Seasonality

The total moisture contribution (combined ABL and FT) from different oceanic regions varies both seasonally and interannually, and a clear contrast in the seasonality of Indian versus Pacific Ocean contributions to EASM rainfall is apparent (Figure 7). Nonmonsoon season moisture uptake from the northern Indian Ocean is low (less than 5 mm month^{-1}) and increases rapidly after ISM onset (up to 20 mm month^{-1}) then decreases following peak EASM activity. Northwest and northeast Indian Ocean contributions are in-phase with the EASM, and the area-weighted northwest Indian Ocean contribution is higher due to uptake from the western Indian Ocean (Figure 3). South China Sea uptake minima, unlike those of the other oceanic source regions, never reach near-zero values during the study period; a small moisture contribution (~7 mm month^{-1}) to the farthest southeastern (coastal) areas of China and to Taiwan is therefore entrained during northward ASM advancement (Figures 3 and 7). These observations are consistent with the available satellite-based scatterometry data, which show precipitation across China and Indochina are generally in-phase with Indian Ocean evaporation [*Liu and Tang*, 2004]. Philippine Sea contributions exhibit limited seasonality, and peak South China Sea contributions occur during winter months. The combined ABL moisture uptake and FT contributions from the northern Indian and northwest Pacific Oceans are summarized in Figure S3 in the supporting information (see also Table S7 in the supporting information). Zonal moisture advection from the Indian Ocean increases rapidly at the point of ASM onset, with maxima during June and July. Total Pacific Ocean contributions (combining the South China and Philippine Seas)

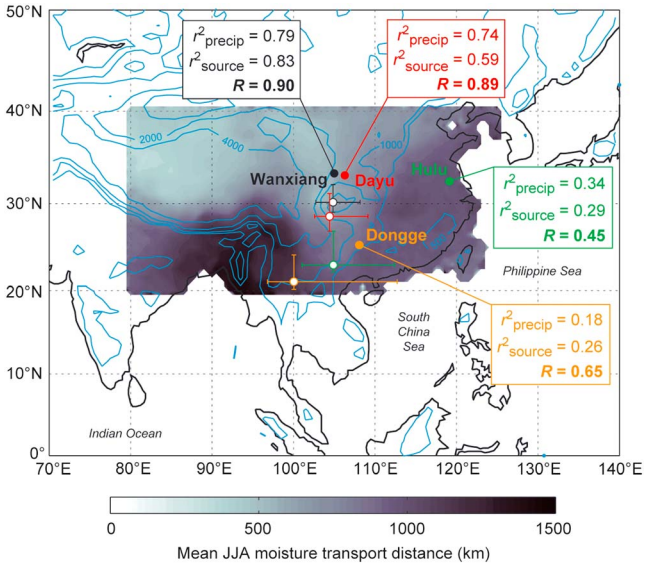

Figure 8. Map of selected cave sites (filled circles), their respective mean June to August moisture source locations (open circles), and moisture source-weighted mean annual range (bars). Contoured data (grey scale) show the modeled mean June to August moisture transport distance (km) from uptake location to precipitation location. Correlation coefficients (r^2) for mean monthly precipitation $\delta^{18}O$ versus mean precipitation amount (r^2_{precip}) and specific humidity-weighted mean moisture source longitude and latitude (r^2_{source}) for the four selected cave sites are given. Also shown is the multivariate r^2 for precipitation $\delta^{18}O$ against amount, source longitude, and source latitude (R), which is geographically variable and higher than individual amount and source correlations at each site. Topographic contours (pale blue) are in meters above mean sea level.

exhibit comparatively limited seasonality (Figure S3 and Table S7 in the supporting information), with two anomalously high values of Pacific moisture export in December 1999 and December 2001.

Moisture exported to monsoonal China from the identified source regions is subsequently recycled, inducing terrestrial moisture fluxes. This terrestrially derived, recycled moisture constitutes a substantial contribution to total precipitation across central and eastern China, particularly during the EASM (Figure 7). Precipitation recycling, estimated here as the percentage of ABL moisture uptake (principally via evapotranspiration) from all terrestrial sources, exhibits no clear seasonality (Figure 7a). Moreover, no clear phase relationship with monthly mean Lagrangian (modeled) precipitation over the target area exists (Figure 7b). Although there is a lack of clear seasonality, due to evaporative terrestrial moisture contributions being present throughout the year (Figure 2), we note that summer values tend to be lower during the examined period, resulting from increased relative moisture contributions from distal oceanic sources. The mean annual terrestrial moisture uptake is 62 mm month^{-1}, which represents a substantial contribution (74.2%) to precipitation over central and eastern China.

3.6. Geographically Variable Source Effect in EASM Precipitation $\delta^{18}O$

Moisture transport processes strongly affect precipitation (and therefore proxy) $\delta^{18}O$ [*Lachniet*, 2009; *Pausata et al.*, 2011]. Reliable paleomonsoon reconstructions from speleothem $\delta^{18}O$ require a detailed understanding of amount effect variability [*Dayem et al.*, 2010], extraregional forcings (e.g., oceanic source conditions) [*Lewis et al.*, 2010; *Pausata et al.*, 2011], and moisture source variability [*Breitenbach et al.*, 2010]. We report here an initial attempt to evaluate variability in the expression of source effects by precipitation $\delta^{18}O$ (see supporting information) at Hulu, Dongge, Wanxiang, and Dayu Caves (Figure 1) by running the Lagrangian diagnostic with additional 2° × 2° target areas centered on each selected cave site (Figure 1 and Table S3 in the supporting information). Our goal is not to quantify absolutely the extent to which source effects explain total precipitation $\delta^{18}O$ variability at the selected sites but instead to assess whether any geographic variability exists. We calculated correlation coefficients between mean monthly precipitation $\delta^{18}O$ and the following predictor variables: mean monthly precipitation amount and specific humidity-weighted source longitude and source latitude. The correlation coefficients r^2_{precip} and r^2_{source} represent regression between precipitation $\delta^{18}O$ and precipitation amount and between $\delta^{18}O$ and specific humidity-weighted mean source location (longitude and latitude), respectively. R denotes the multivariate correlation coefficient for precipitation $\delta^{18}O$ regressed against mean monthly amount, source longitude, and source latitude (Figure 8).

We observe a spatially variable source effect between the selected cave sites (Figure 8), as indicated by mean source longitude and latitude data. For each site, a combination of precipitation amount, source longitude, and source latitude explains a greater degree of precipitation $\delta^{18}O$ variability than individual site-specific amount or source effects alone (Figure 8). This is particularly true for Hulu, where amount and source

effects appear similarly important (34% and 29%, respectively), and for Dongge, where individual amount and source effects explain only a limited proportion of the precipitation $\delta^{18}O$ variability (18% and 26%, respectively). Precipitation $\delta^{18}O$ variance not explained by amount and source effects for the selected sites is likely due to the influence of other hydroclimatic parameters, such as cloud temperature or convective intensity [*Risi et al*., 2008], which require further investigation in future studies focused on monsoonal China. Nevertheless, these results indicate that precipitation $\delta^{18}O$ across monsoonal China integrates a significant and geographically variable source signal.

Northeast India and the Ganges-Brahmaputra deltaic region receive moisture transported over the greatest mean distance from the Indian Ocean (Figures 3 and 4). In the EASM region, a southeast-northwest gradient in moisture transport distance exists (Figure 8). Mean source regions for EASM precipitation at Hulu and Dongge are located ~1700 and ~1000 km southwest of each site, respectively, and for Dayu and Wanxiang, ~500 and ~400 km south, respectively. Raw moisture uptake data (within the ABL) are given in Table S8 in the supporting information). Each site predominantly receives moisture advected from the west, and the relative proximity of the northern Dayu and Wanxiang sites to their mean source regions demonstrates that they receive a greater proportion of recycled moisture, where mean June to August moisture transport distance is relatively short (Figure 8). The intensity of summer moisture recycling apparent within monsoonal China exceeds that over northeast India, where mean moisture transport distance is higher. (Note that the lowest moisture transport distance values are found over the Tibetan Plateau.) However, our results show no obvious "transitional zone" between the ISM and EASM regions [*Wang and Lin*, 2002], instead evincing strong westerly moisture transport across continental eastern Asia, predominantly from the Indian Ocean domain.

4. Conclusions

In summary, we quantified the seasonal progression of evaporative moisture contributions to precipitation across central and eastern China from the Indian and Pacific Oceans, comprising a subcontinental-scale investigation of moisture transport to the world's most populous monsoonal region. The seasonal cycle of moisture sources shows a rapid transition from a dry winter period, with predominately easterly moisture contributions, to an intense summer monsoon phase, with extensive contributions from the northern Indian Ocean and moisture recycling over continental areas. Modeled precipitation data accurately reproduce the observed climatological EASM precipitation distribution across southern and eastern China, firmly substantiating the diagnosed moisture transport patterns. Despite distinct differences in the onset and characteristics of the monsoon season over India, eastern China, and the western North Pacific [*Wang and Lin*, 2002], the Indian Ocean moisture contribution to EASM precipitation in China is considerable. These results present a significant challenge to the previously assumed Pacific Ocean origin for EASM precipitation in China [e.g., *Ran and Feng*, 2013; *Xu et al*., 2004], are entirely consistent with ISM-EASM mechanistic linkage [*Cheng et al*., 2012], and provide a highly plausible explanation for precipitation proxy covariation between China and India during late Holocene warm phases [*Rehfeld et al*., 2013].

Interestingly, our data show that transport of rain-bearing moisture from the northwestern and low-latitude Pacific Ocean during the EASM is minimal and largely indistinguishable from that during winter (Figure 3). Additionally, we detected no significant contribution to EASM rainfall from the high-latitude Westerlies, previously indicated by a smaller-scale analysis [*Liu et al*., 2014]. Rather, the results of this study quantify a significant Indian Ocean contribution across the EASM region, predominately originating from the northern Indian Ocean, and demonstrate that zonal westerly advection reaches China's eastern continental margin and the wettest southern region during peak EASM (Figures 3 and 4). The spatial extent of Pacific Ocean moisture contributions is comparatively limited and seasonally invariant (Figures 3 and 7); Pacific free tropospheric convective moistening is also less widespread than that over Indian Ocean regions (Figure 4).

General circulation model (GCM) studies project significant anthropogenic CO_2-induced warming over the tropical oceans [*IPCC*, 2013], one consequence of which is lower atmosphere moisture budget increase [*Hsu et al*., 2013; *Lee and Wang*, 2014; *Ueda et al*., 2006]. Considering this, our results indicate that changes in Indian Ocean, rather than Pacific Ocean, sea surface temperature and moisture export will directly influence future EASM rainfall variability across central and eastern China. Given the projected increase in

the geographical Asian monsoonal domain [*Lee and Wang*, 2014], quantifying the EASM precipitation response to Indian Ocean surface warming is an important area for future research.

The expression of the source effect in modern precipitation $\delta^{18}O$ within monsoonal China is significant and varies in strength between the Hulu, Dongge, Dayu, and Wanxiang Cave sites, which is most likely due to differences in mean moisture transport distance during summer. Precipitation $\delta^{18}O$ at each site is more accurately interpreted as reflecting both rainfall amount and moisture transport history. Given our data and existing GCM evidence for a strong response of precipitation $\delta^{18}O$ across China to upstream rainout [*Liu et al.*, 2014; *Pausata et al.*, 2011], it is now increasingly clear that $\delta^{18}O$ does not directly and exclusively record local precipitation variability at sites within monsoonal China. Our moisture source data provide a widely applicable basis for quantifying source effects in precipitation and proxy $\delta^{18}O$, thereby isolating local or regional precipitation amount signals that are crucial for accurate paleomonsoon reconstruction.

Acknowledgments

This research was funded by a Durham University Sir Kingsley Dunham Studentship awarded to A.J.B., a National Natural Science Foundation of China grant (41273014) awarded to K.R.J. and P.Z., and a Swiss National Foundation (Sinergia grant CRSI22-132646/1) awarded to S.F.M.B. We thank A. Stohl for providing the FLEXPART data set and two anonymous reviewers whose comments much improved the first draft of this paper. Raw data are provided in the supporting information or available from A.J.B. (a.j.baker@durham.ac.uk) upon request.

References

Breitenbach, S. F. M., J. F. Adkins, H. Meyer, N. Marwan, K. K. Kumar, and G. H. Haug (2010), Strong influence of water vapor source dynamics on stable isotopes in precipitation observed in Southern Meghalaya, NE India, *Earth Planet. Sci. Lett.*, *292*, 212–220.

Chen, B., X.-D. Xu, and T. Zhao (2013), Main moisture sources affecting lower Yangtze River Basin in boreal summers during 2004–2009, *Int. J. Climatol.*, *33*, 1035–1046.

Cheng, H., R. L. Edwards, W. S. Broecker, G. H. Denton, X. G. Kong, Y. J. Wang, R. Zhang, and X. F. Wang (2009), Ice Age terminations, *Science*, *326*, 248–252.

Cheng, H., A. Sinha, X. Wang, F. Cruz, and R. L. Edwards (2012), The global paleomonsoon as seen through speleothem records from Asia and the Americas, *Clim. Dyn.*, *39*, 1045–1062.

Clemens, S. C., W. L. Prell, and Y. B. Sun (2010), Orbital-scale timing and mechanisms driving late Pleistocene Indo-Asian summer monsoons: Reinterpreting cave speleothem $\delta^{18}O$, *Paleoceanography*, *25*, PA4207, doi:10.1029/2011PA002268.

Cosford, J., H. R. Qing, B. Eglington, D. Mattey, D. X. Yuan, M. L. Zhang, and H. Cheng (2008), East Asian monsoon variability since the mid-Holocene recorded in a high-resolution, absolute-dated aragonite speleothem from eastern China, *Earth Planet. Sci. Lett.*, *275*, 296–307.

Dayem, K. E., P. Molnar, D. S. Battisti, and G. H. Roe (2010), Lessons learned from oxygen isotopes in modern precipitation applied to interpretation of speleothem records of paleoclimate from eastern Asia, *Earth Planet. Sci. Lett.*, *295*, 219–230.

Ding, Y., and D. R. Sikka (2006), Synoptic systems and weather, in *The Asian Monsoon*, edited by B. Wang, pp. 131–201, Praxis Springer, Berlin.

Ding, Y. H., C. Y. Li, and Y. J. Liu (2004), Overview of the South China Sea monsoon experiment, *Adv. Atmos. Sci.*, *21*, 343–360.

Gimeno, L., A. Drumond, R. Nieto, R. M. Trigo, and A. Stohl (2010), On the origin of continental precipitation, *Geophys. Res. Lett.*, *37*, L13804, doi:10.1029/2010GL043712.

Helsen, M. M., R. S. W. Van de Wal, and M. R. Van den Broeke (2007), The isotopic composition of present-day Antarctic snow in a Lagrangian atmospheric simulation, *J. Clim.*, *20*, 739–756.

Hsu, P.-C., T. Li, H. Murakami, and A. Kitoh (2013), Future change of the global monsoon revealed from 19 CMIP5 models, *J. Geophys. Res. Atmos.*, *118*, 1247–1260.

Hu, C. Y., G. M. Henderson, J. H. Huang, S. Xie, Y. Sun, and K. R. Johnson (2008), Quantification of Holocene Asian monsoon rainfall from spatially separated cave records, *Earth Planet. Sci. Lett.*, *266*, 221–232.

IAEA/WMO (2014), Global Network of Isotopes in Precipitation, The GNIP Database.

Intergovernmental Panel on Climate Change (IPCC) (2013), *Climate Change 2013: The Physical Science Basis. Contribution of Working Group I to the Fifth Assessment Report of the Intergovernmental Panel on Climate Change*, edited by T. F. Stocker et al., pp. 1535, Cambridge Univ. Press, Cambridge, U. K., and New York, doi:10.1017/CBO9781107415324.

James, P., A. Stohl, N. Spichtinger, S. Eckhardt, and C. Forster (2004), Climatological aspects of the extreme European rainfall of August 2002 and a trajectory method for estimating the associated evaporative source regions, *Nat. Hazards Earth Syst. Sci.*, *4*, 733–746.

Johnson, K. R., and B. L. Ingram (2004), Spatial and temporal variability in the stable isotope systematics of modern precipitation in China: Implications for paleoclimate reconstructions, *Earth Planet. Sci. Lett.*, *220*, 365–377.

Kennett, D. J., et al. (2012), Development and disintegration of Maya political systems in response to climate change, *Science*, *338*, 788–791.

Lachniet, M. S. (2009), Climatic and environmental controls on speleothem oxygen-isotope values, *Quat. Sci. Rev.*, *28*, 412–432.

Lee, J.-Y., and B. Wang (2014), Future change of global monsoon in the CMIP5, *Clim. Dyn.*, *42*, 101–119.

Legates, D. R., and C. J. Willmott (1990), Mean seasonal and spatial variability in gauge-corrected, global precipitation, *Int. J. Climatol.*, *10*, 111–127.

Lewis, S. C., A. N. LeGrande, M. Kelley, and G. A. Schmidt (2010), Water vapour source impacts on oxygen isotope variability in tropical precipitation during Heinrich events, *Clim. Past.*, *6*, 325–343.

Li, Y., N. A. Wang, X. Zhou, C. Zhang, and Y. Wang (2014), Synchronous or asynchronous Holocene Indian and East Asian summer monsoon evolution: A synthesis on Holocene Asian summer monsoon simulations, records and modern monsoon indices, *Global Planet. Change*, *116*, 30–40.

Liu, J. R., X. F. Song, G. B. Fu, X. Liu, Y. H. Zhang, and D. M. Han (2011), Precipitation isotope characteristics and climatic controls at a continental and an island site in Northeast Asia, *Clim. Res.*, *49*, 29–44.

Liu, W. T., and W. Tang (2004), Oceanic influence on the precipitation in India and China as observed by TRMM and QuikSCAT, in *The 2nd International Tropical Rainfall Measuring Mission Science Conference*, Jpn. Aerosp. Explor. Agency, Tokyo.

Liu, Z., et al. (2014), Chinese cave records and the East Asia summer monsoon, *Quat. Sci. Rev.*, *83*, 115–128.

Maher, B. A., and R. Thompson (2012), Oxygen isotopes from Chinese caves: Records not of monsoon rainfall but of circulation regime, *J. Quat. Sci.*, *27*, 615–624.

Martius, O., et al. (2013), The role of upper-level dynamics and surface processes for the Pakistan flood of July 2010, *Quat. J. R. Meteorol. Soc.*, *139*, 1780–1797.

Molnar, P., W. R. Boos, and D. S. Battisti (2010), Orographic controls on climate and paleoclimate of Asia: Thermal and mechanical roles for the Tibetan Plateau, *Ann. Rev. Earth Planet. Sci.*, *38*, 77–102.

Pausata, F. S. R., D. S. Battisti, K. H. Nisancioglu, and C. M. Bitz (2011), Chinese stalagmite $\delta^{18}O$ controlled by changes in the Indian monsoon during a simulated Heinrich event, *Nat. Geosci.*, *4*, 474–480.

Ran, M., and Z. Feng (2013), Holocene moisture variations across China and driving mechanisms: A synthesis of climatic records, *Quat. Int.*, *313–314*, 179–193.

Rehfeld, K., N. Marwan, S. M. Breitenbach, and J. Kurths (2013), Late Holocene Asian summer monsoon dynamics from small but complex networks of paleoclimate data, *Clim. Dyn.*, *41*, 3–19.

Risi, C., S. Bony, and F. Vimeux (2008), Influence of convective processes on the isotopic composition ($\delta^{18}O$ and δD) of precipitation and water vapor in the tropics: 2. Physical interpretation of the amount effect, *J. Geophys. Res.*, *113*, D19306, doi:10.1029/2008JD009943.

Rozanski, K., L. Araguás-Araguás, and R. Gonfiantini (1992), Relation between long-term trends of oxygen-18 isotope composition of precipitation and climate, *Science*, *258*, 981–985.

Sampe, T., and S.-P. Xie (2010), Large-scale dynamics of the Meiyu-Baiu rainband: Environmental forcing by the westerly jet, *J. Clim.*, *23*, 113–134.

Schneider, T., T. Bischoff, and G. H. Haug (2014), Migrations and dynamics of the intertropical convergence zone, *Nature*, *513*, 45–53.

Schneider, U., A. Becker, P. Finger, A. Meyer-Christoffer, B. Rudolf, and M. Ziese (2011), Global precipitation climatology center full data reanalysis version 6.0 at 1.0°: Monthly land-surface precipitation from rain-gauges built on GTS-based and historic data, Deutscher Wetterdienst, doi:10.5676/DWD_GPCC/FD_M_V6_100.

Sodemann, H., and A. Stohl (2009), Asymmetries in the moisture origin of Antarctic precipitation, *Geophys. Res. Lett.*, *36*, L22803, doi:10.1029/2009GL040242.

Sodemann, H., and E. Zubler (2010), Seasonal and interannual variability of the moisture sources for Alpine precipitation during 1995–2002, *Int. J. Climatol.*, *30*, 947–961.

Sodemann, H., V. Masson-Delmotte, C. Schwierz, B. M. Vinther, and H. Wernli (2008a), Interannual variability of Greenland winter precipitation sources: 2. Effects of North Atlantic Oscillation variability on stable isotopes in precipitation, *J. Geophys. Res.*, *113*, D12111, doi:10.1029/2007JD009416.

Sodemann, H., C. Schwierz, and H. Wernli (2008b), Interannual variability of Greenland winter precipitation sources: Lagrangian moisture diagnostic and North Atlantic Oscillation influence, *J. Geophys. Res.*, *113*, D03107, doi:10.1029/2007JD008503.

Stohl, A. (2006), Characteristics of atmospheric transport into the Arctic troposphere, *J. Geophys. Res.*, *111*, D11306, doi:10.1029/2005JD006888.

Stohl, A., C. Forster, A. Frank, P. Seibert, and G. Wotawa (2005), Technical note: The Lagrangian particle dispersion model FLEXPART version 6.2, *Atmos. Chem. Phys.*, *5*, 2461–2474.

Tan, L., Y. J. Cai, H. Cheng, Z. S. An, and R. L. Edwards (2009), Summer monsoon precipitation variations in central China over the past 750 years derived from a high-resolution absolute-dated stalagmite, *Palaeogeog., Palaeoclimatol., Palaeoecol.*, *280*, 432–439.

Ueda, H., A. Iwai, K. Kuwako, and M. E. Hori (2006), Impact of anthropogenic forcing on the Asian summer monsoon as simulated by eight GCMs, *Geophys. Res. Lett.*, *33*, L06703, doi:10.1029/2005GL025336.

van der Ent, R. J., and H. H. G. Savenije (2013), Oceanic sources of continental precipitation and the correlation with sea surface temperature, *Water Resour. Res.*, *49*, 3993–4004, doi:10.1002/wrcr.20296.

Wang, B., and H. Lin (2002), Rainy season of the Asian-Pacific summer monsoon, *J. Clim.*, *15*, 386–398.

Wang, Y. J., H. Cheng, R. L. Edwards, Z. S. An, J. Y. Wu, C. C. Shen, and J. A. Dorale (2001), A high-resolution absolute-dated late Pleistocene monsoon record from Hulu Cave, China, *Science*, *294*, 2345–2348.

Webster, P. J., V. O. Magana, T. N. Palmer, J. Shukla, R. A. Tomas, M. Yanai, and T. Yasunari (1998), Monsoons: Processes, predictability, and the prospects for prediction, *J. Geophys. Res.*, *103*, 14,451–14,510, doi:10.1029/97JC02719.

Xu, X. D., L. S. Chen, X. R. Wang, Q. J. Miao, and S. Y. Tao (2004), Moisture transport source/sink structure of the Meiyu rain belt along the Yangtze River valley, *Chin. Sci. Bull.*, *49*, 181–188.

Zhang, P. Z., et al. (2008), A test of climate, Sun, and culture relationships from an 1810-year Chinese cave record, *Science*, *322*, 940–942.